University of Tehran Press

Online ISSN: 2345-475X

DESERT

Home page: https://jdesert.ut.ac.ir/

Monitoring the spatial autocorrelation of land surface temperature with land use in different climatic regions (Case Study: The Metropolitans of Mashhad and Sari)

Zinat Komeh[1], Saeid Hamzeh[1], Hadi Memarian[2], Sara Attarchi[1], Seyed Kazem Alavipanah[1*]

[1*] Department of Remote Sensing and GIS, University of Tehran, Tehran, Iran. E-mail: salavipa@ut.ac.ir
[2] Department of Watershed Management, Faculty of Natural Resources and Environment, University of Birjand, Birjand, Iran.

Article Info.

Article type:
Research Article

Article history:
Received: 04 Jun. 2023
Received in revised from: 14 Aug. 2023
Accepted: 15 Sep. 2023
Published online: 27 Dec. 2023

Keywords:
Google Earth Engine,
Hot Spots,
Temperature changes,
Land use changes.

ABSTRACT

Knowing the temporal and spatial changes of land use and the formation of heat islands over time is one of the most important issues in metropolitan planning and policy making. Thus, in this study heat islands and temperature changes and its relationship with land use changes have been monitored over a period of 35 years in two study areas, i.e. the cities of Mashhad and Sari, using the Google Earth Engine platform. For this purpose, the LST was computed and the land use maps of the studied periods were extracted during 8 time steps of 5 years from 1985 to 2020. The aim of this study is to investigate the spatial autocorrelation of heat islands and its relationship with land use in two studied regions with different climatic conditions. The results of temperature monitoring showed an increase in temperature between 1 to 2 °C in all types of land uses during 35 years. This increasing trend of temperature is proportional to the type of land use changes, so that the temperature increase in built-up lands was estimated to be 2 and 1.75 degrees Celsius in the cities of Sari and Mashhad, respectively. The average temperature of the three months of summer in Mashhad city in built-up areas has increased from 34.5°C to 36.25°C and in Sari city from 29.51°C to 31.51°C. while the minimum increase in temperature has occurred in the lands with forest coverage, which is 1.02 °C and 1.19 °C, respectively in the cities of Sari and Mashhad. Conclusively, in both climatic regions, the areas where the changes are in the direction of reducing or removing vegetation and creating residential areas, the temperature increase is the maximum, and the areas where the changes are in the direction of increasing forests and agricultural lands, the temperature increase is the minimum.

Cite this article: Komeh, Z., Hamzeh, S., Memarian, H., Attarchi, S., Alavipanah, S.K. (2023). Monitoring the Spatial Autocorrelation of Land Surface Temperature with Land Use in Different Climatic Regions (Case Study: The Metropolitans of Mashhad and Sari). DESERT, 28 (2), DOI: 10.22059/jdesert.2023.95643

DOI: 10.22059/jdesert.2023.95643

Publisher: University of Tehran Press

1. Introduction

Considering that during the past half century, the surface of the earth has undergone many changes due to human activities through deforestation and the development of cities, knowing the ratio of land uses and how it changes over time is one of the most important things in planning and it is urban policies (Asghari and Emami, 2018). Given that the LST (Land Surface Temperature) is significantly affected by the type of land use and land cover, therefore it can be considered correctedan import ant factor in global warming studies and as a proxy for climate change. The change in LST is also an intuitive regional climate response to global climate change and is of great importance in agriculture, hydrology, ecology, environment, climate and biogeochemistry and directly causes changes in the properties that becomes the surface of the earth (Tan *et al.*, 2020). For this reason, the rapid changes in land use have become a major environmental concern and also the cause of many problems, including the reduction of green space and the development of heat islands (Amiri *et al.*, 2009). Moreover, it has had several impacts on the surface temperature on a local to global scale (Hamzeh *et al.*, 2018, Xiao, *et al.*, 2022). It is also mentioned as one of the most urgent problems among scientists around the world, that experts warn about it and even mention it as an incomprehensible torment of mankind (Alavipanah *et al.*, 2022). The urban heat islands and surface emissivity are important indicators in the study of energy balance models on the earth's surface and the investigation of earth surface interactions on a regional and global scale (Zandi *et al.*, 2023). During the past half a century, the land surface has undergone many changes due to human activities through deforestation and urban development (Owen *et al.*, 1998). Therefore, examining the relationship between land use and surface temperature with an accurate method and taking into account the influencing variables can provide truthful results to assist urban planning managers, who have so far conducted many studies to investigate this issue inside and outside the country. Thus far, the basis of various factors has been studied, as well (Estoque *et al.* 2017; Shi *et al.* 2017; Kazemi *et al.*, 2018; and Zandi *et al.*, 2014).

Stock *et al.* (2017) in the big cities of Bangkok (Thailand), Jakarta (Indonesia) and Manila (Philippines) investigated the relationship between surface temperature and the frequency/pattern of impervious surface space and green space. The results demonstrate a strong significant relationship between the mean LST and the density of impervious surface (positive relationship) and green space (negative relationship) along the urban-rural slope of three cities. Furthermore, the relationship between impervious surface density and average LST showed an increasing trend in larger networks, while the relationship between green space density and average LST showed a tendency to increase in smaller networks which shows the strong influence of impervious surface and green space on the variation of LST in larger and smaller areas, respectively.

Shi *et al.* (2017) modeled the effects of the spatial-temporal pattern of urban heat islands using the land use regression approach. The findings of this research showed that the spatial pattern of urban heat islands is highly determined by land use and land cover maps and urban geomorphology metrics, and the resulting models are used to enrich current urban design agendas and help to deal with urban heat islands. Tran *et al.* (2017) investigated the relationship between LST and land cover change using Landsat images. Their results showed that the LST has a non-linear relationship with the types of earth's surface cover, and the analysis of the Getis–Ord Gi index (GI) allows the analysis of the change of surface temperature pattern over time. Wang *et al.* (2018) investigated land use changes and their impact on LST changes in Yangon, Myanmar. The results of this study established that the alterations in land use have complex and direct effects on changes of the LST, so that urban areas show the highest surface temperature. Feng *et al.* (2019) investigated the relationship between changes in LST with three

factors: normalized difference vegetation index (NDVI), normalized difference built-up index (NDBI) and normalized difference water index (NDWI) and reported that the LST surface is strongly influenced by the mentioned three factors.

He *et al.* (2019) studied the effects of terrestrial factors on LST using Landsat 8 images in mountainous regions of China. The results showed that there is an inverse relationship between the altitude and the angle of the sun's radiation with the surface temperature. Moreover, in the southern directions, the surface temperature changes were more than in other directions, and vegetation was the key factor affecting the surface temperature changes. Wang *et al.* (2019) also investigated land use changes and LST in the Pearl River Delta in China over time in another study. Their results showed that the growth of the city in this area and the surface temperature patterns have increased with the destruction of some land uses. Tan *et al.* (2020) investigated the spatial relationship between land use/land cover changes and LST in the Dongying Lake region of China using Landsat 7 satellite images. They stated that the results of correlation analysis indicate that vegetation cover, air humidity and distance from water bodies can regulate surface temperature significantly. They also investigated the relationship between LST and other factors (i.e. NDVI, Normalized Difference Moisture Index (NDMI), DEM and proximity to water bodies). In terms of the correlation between the average LST and those factors, NDMI has the greatest effect on the changes of LST, followed by the proximity to water bodies, NDVI and DEM. Furthermore, the winter LST in the study area increased by approximately 3.5°C, which may be related to the decrease in the acreage of Dongying Lake. Alavipanah *et al.* (2022) in a study investigated the side effects of global warming as well as the main cause of global warming. They proved that global warming itself causes additional global warming. In a study, Zandi *et al.* (2023) measured the spatial autocorrelation of LST with land use in Isfahan city, Iran. They analyzed the urban heat island effect using data from the OLI (Operational Land Imager) of the Landsat satellite. According to results, there was a clustering in the LST with a 99% confidence level, thus they examined the hot and cold spots. Their results showed that thermal islands have a direct and incremental relationship with built-up and barren land uses and an inverse relationship with water bodies and vegetative uses.

Tajbakhsh *et al.* (2017) analyzed and modeled urban expansion and land use changes in Mashhad city from 1967 to 2015 and finally simulated the upcoming changes for 2025 in a study using Cellular Automata- Markov model. The results showed that with the physical expansion of continuous urban patches, pasture lands and agricultural lands mainly turned into discontinuous urban patches and eventually joined the continuous urban fabric. They stated that this process of changes and transformations in urbanization spots will lead to the loss of agricultural lands and rangeland of Mashhad in 2025. Moreover, the analysis of the predicted land use map indicated that in the coming years, the development of the city in the northern front, especially in the northwest region, will take place at a higher speed than in other regions. The results of a research conducted by Alavipanah *et al.* (2014) in order to analyze the spatio-temporal changes of thermal islands of Mashhad city with regard to the expansion of the city and changes in land use and land cover showed that about 2500 hectares of agricultural lands and green spaces converted to built-up areas that will lead to the hot spots of temperature. This shows that the reduction of vegetation has been the most important factor in the expansion of thermal islands in Mashhad. Likewise, in a similar study, Abdi *et al.* (2021) investigated the role of urban green space coverage on the temperature changes in the city of Sari using the Landsat 7 and 8 satellite images of 2009, 2013 and 2017. Their results indicate that the central area of the city, which is less suitable in terms of the coverage and distribution of green space than other areas of the city is warmer. They also announced that the LST during the statistical period had an upward trend in the minimum and maximum conditions that was less seen in the

areas of the city which had more green spaces. Based on the outcomes, in the future years, these regions can play a moderating role in the surface temperature of the city.

Therefore, this study was aimed to monitor and compare the degree of spatial autocorrelation of the LST, and its relationship with land use in two regions with different climatic conditions, and different density/type of vegetation cover which are very heterogeneous and distinct from each other in terms of land use and land cover characteristics. This work was carried out over a period of 35 years in order to compare the difference between the changes in the studied regions with different climates and discussed the trends of these alterations in the transformed land uses. For this purpose, first by classifying satellite images, the land use map has been extracted in each period for both regions. Then, by preparing a map of the LST, the pattern governing the LST and the monitoring of the spatial autocorrelation of the temperature of the surface of the earth with land use and the changes made during the period of 35 years have been investigated.

2. Materials and methods

2.1. Study area

In this study, two regions with different climatic conditions and vegetation density, namely the cities of Mashhad and Sari and their surrounding areas, have been used to compare the environmental conditions. Both studied areas include urban and suburban areas, which are very heterogeneous and distinct from each other in terms of land use and land cover characteristics. The city of Sari, located in the foothills of the Alborz mountain range, involves two mountainous and plain parts, which are located in the geographical range of 53º0′44″ to 53º07′47″ east and 36º30′7″ to 36º35′50″ north, with a mean altitude of 54 meters above sea level. The climate of Sari is moderate Caspian which is mild and humid in summers and relatively cold and humid in winters. The southern mountainous parts of this city have long and very cold winters, as well. During the last few years, the coldest temperature of this city has been recorded by -12 °C in winter and +40 °C in summer. The city of Mashhad is located in the basin of the Kashfroud river and in the Mashhad plain between the mountains of Hezar Masjid and Binaloud in the geographical range of 59º26′5″ to 53º43′36″ east and 36º10′42″ to 36º24′12″ north. The maximum altitude of Mashhad city is 1150 meters and the minimum is 950 meters. The city of Mashhad has a variable climate, but it is moderate and tends to be cold and dry with hot/dry summers and cold/wet winters. Its maximum temperature in summer is 43°C and the minimum temperature in winter is -23°C.

2.2. Data and Methodology

In this study, the Google Earth Engine system as a cloud platform was employed to process the time series of satellite data, with the necessary pre-processing and microscaling, as well as the classification of satellite images, preparation of land use maps, validity measurement, required post-processing by applying necessary filters, and the preparation of LST maps. This system is a web-based remote sensing platform with the ability to perform spatial and temporal calculations on more than one set of satellite images and enables users to perform their computations on a large amount of data without the need for a system (Kumar and Mutanga, 2018; Sidhu *et al.*, 2018). With the availability of Google Earth Engine, the daily, monthly, seasonal and long-term monitoring of phenomena with high spatial resolution on a wide scale has been possible (Monanga and Kumar, 2019) and many limitations of loading, storage and processing data that occurs when working with large land cover data is resolved (Ravanelli *et al.*, 2018; Gorelick *et al.*, 2017; Nascetti *et al.*, 2017). This system supports all types of commonly used satellite images, such as Landsat, Sentinel, Aster, Modis, etc. In this study, the

series of Landsat satellite images have been employed due to having appropriate spectral, spatial and temporal resolution, and a complete archive of these imageries in the studied period by the United States Geological Survey. In this work, in order to avoid the effects of seasonal changes, the average imageries of May, June and July with less than 5% cloud cover were selected to extract land use/cover maps (Table 1).

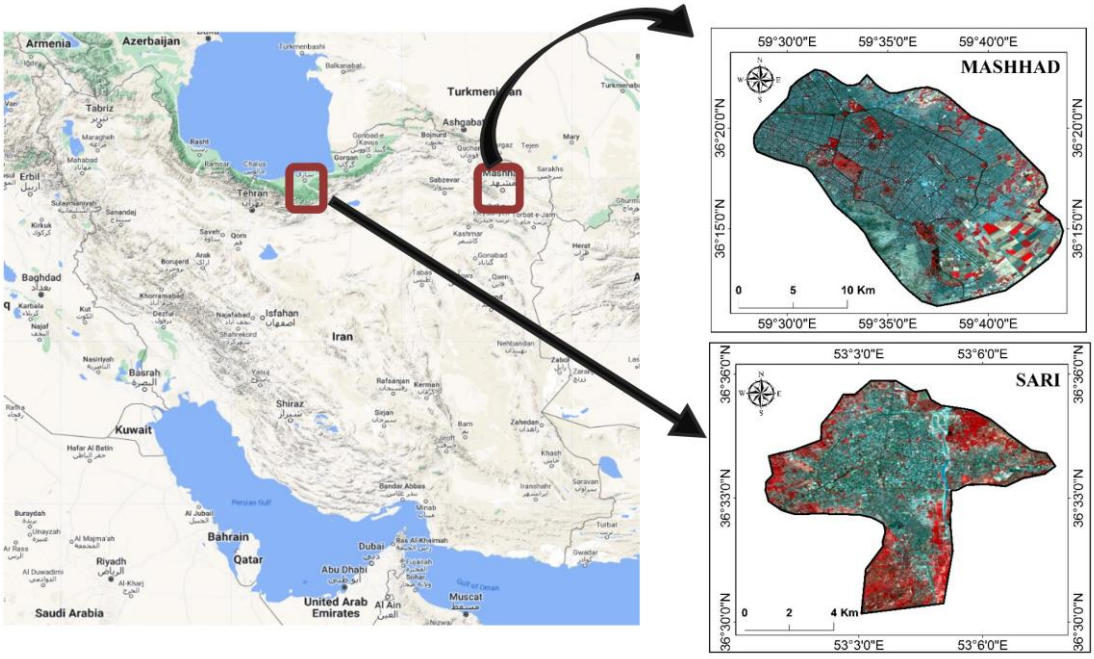

Fig. 1. OLI sensor images of Landsat 8 satellite, with band combination 5, 4, 3 of the studied areas, dated 2020

Table 1. Images used in this study.

	SATELLITE	SENSOR		
Land Use & LST	Landsat 5	TM	1985, 1990, 1995	1985-1990 1990-1995
	Landsat 7	ETM^{+}	2000, 2005, 2010	1995-2000 2000-2005 2005-2010
	Landsat 8	OLI	2015, 2020	2010-2015 2015-2020

- **Land use classification**

In order to prepare the land use map, the object-oriented classification approach was used, which has a much higher accuracy than the common pixel based methods (Memarian et al, 2013; Li *et al.*, 2016; Zaretkar *et al.*, 2019) by using the Support Vector Machine (SVM) algorithm, with defining 6 classes of built up areas, water body, agriculture, forest and green space, rangelands and barren. In the object-oriented method, image classification is based on texture, dimensions, and specific patterns, and instead of sampling a single pixel, the shape and structure of the complication pattern is sampled. In this method, the pixels of a region with the same spectral and spatial characteristics form a separate unit is called a segment. In general, this method consists of two processes of segmentation and classification (Yan, 2003). In the process of segmentation,

objects on the image level are divided based on the spatial and spectral separation of images by a group of pixels according to the spectral and geometric characteristics determined by the observer (Agarwal *et al.*, 2013). Then the classification is done based on the determined algorithms, i.e. the support vector machine algorithm in this work, and the produced parts are classified into classes with the same characteristics. In the support vector machine algorithm, after selecting the segmentation levels and based on the selected ground samples, the classification is accomplished based on the assumptions in the support vector machine algorithm. This algorithm has received a lot of attention because it does not depend on a special statistical distribution and has high accuracy in classification, and it is considered a very powerful algorithm in the object-oriented method, especially in the areas where complications are heterogeneous (Gao *et al.*, 2009; Mackie *et al.*, 2013; Puissant *et al.*, 2014; Petropoulos *et al.*, 2014).

- **Land surface temperature (LST) extraction**

The LST is a function of net energy on the land surface, which depends on the amount of energy reaching the land surface, surface emissivity, humidity and air flow of the atmosphere, topography, climatic conditions of the region, which also changes with the change of each of the above parameters (Rott, 2000; Sobrino *et al.*, 1991). In recent years, with the development of remote sensing technology, the LST can be calculated for a large area with high accuracy. The application of thermal infrared radiation and physical model is considered as a suitable tool for calculating the temperature of a wide land surface (Sobrino *et al.*, 2016; Kotchi *et al.*, 2016). Nowadays, the issue of determining the land surface temperature and its suitable methods are of interest to many science researchers. Although different methods have been presented so far, especially for thermal data related to different gauges, the issue of the accuracy of the results is still being evaluated and discussed (Alavipanah *et al.*, 2018). In this study, in order to extract and retrieve the LST, the mono window algorithm was used, and the LST was extracted during the study period in order to check the relationship between LST and land use. In order to calculate the LST using the mono-window algorithm, in addition to the brightness temperature and the emission index and Planck's equation, it is necessary to compute the average air temperature. The application of the mean atmospheric temperature in this equation gives better results for LST (Rongali *et al.*, 2018; Wang *et al.*, 2019-b). The following steps are used to extract the surface temperature and convert it to Celsius based on the mono window method:

The conversion of a digital number to spectral radiation is based on the reference values of spectral radiation provided in the Landsat Guide (Landsat project Science Office, 2002) that can be represented by the following relationship (Abdul Athick *et al.*, 2019):

$$L\lambda = \frac{(L_{MAX} - L_{MIN})}{((QCAL_{MAX} - QCAL_{MIN}))} \times (DN - QCAL_{MIN}) + L_{MIN} \quad (1)$$

In this equation, DN is the digital number of each pixel, L_{MAX} and L_{MIN} are the calibration constants, or in other words, the minimum and maximum radiance values of the thermal band of the sensor, $QCAL_{MAX}$ and $QCAL_{MIN}$ are the largest and smallest digital numbers for band 6 of TM and ETM+ (equal to 255 and 1, respectively), and for band 10 OLI sensor (equal to 65535 and 1, respectively). All of these values are provided in the metadata of the image file.

Conversion of spectral radiance to blackbody temperature: TM, ETM^{+} and OLI thermal band data are converted from spectral radiance to blackbody temperature (TB) using the Planck's relation, assuming a radiant power of one (maximum radiant power) (Abdul Athick *et al.*, 2019):

$$T_B = \frac{k_2}{ln\left(\frac{k_1}{L\lambda}+1\right)} \quad (2)$$

Where, T_B is equal to the effective temperature in the satellite in Kelvin (K), k_1 is the first calibration constant, k_2 is the second calibration constant, and $L\lambda$ is the spectral radiance of the desired pixel (Table 2).

Table 2. Values of K_1, K_2, $QCAL_{MAX}$, $QCAL_{MIN}$ based on the metadata file of the images used

$QCAL_{MIN}$	$QCAL_{MAX}$	K_2	K_1	
255	1	1260.56	607.76	TM
255	1	1282.71	666.09	ETM^+
65535	1	1321.0789	774.8853	OLI/TIRS

- **Emissivity correction**

Diffusion coefficient is the nature of radiative heat transfer, absorption and emission of electromagnetic radiation. One of the parameters that has a great effect on heat transfer by radiation is the emissivity (ϵ) of the radiating body to the receiving body. The diffusion coefficient changes between zero and one. For an object that has no radiation, this coefficient is zero, and for an object that has maximum radiation and actually has the radiation power of a black body, it is one (Alavipanah, 2015). One of the operational and practical options for obtaining radiant power is the vegetation index threshold method, which is defined based on NDVI values and as Table No. 3 (Becker & Li, 1990; Sorbino *et al.*, 2004).

Table 3. Calculation of the radiant power based on determining the vegetation cover index threshold

$\boldsymbol{\varepsilon_{soil} = 0.97}$	The pixel is considered as bare soil	NDVI<0.2
$\varepsilon_{veg} = 0.99$	Pixels are considered as fully vegetated, and then a constant value for the emissivity is assumed.	NDVI>0.5
$\varepsilon = \varepsilon_{veg} p_V + \varepsilon_{soil}(1 - p_V)$	the pixel is composed by a mixture of bare soil and vegetation	0.2≤NDVI≤0.5

In the following equation, Pv is equivalent to vegetation ratio (Sobrino *et al.*, 2004; Carlson & Ripley, 1997):

$$P_V = \left(\frac{NDVI - NDVI_{MIN}}{NDVI_{MAX} - NDVI_{MIN}}\right)^2 \quad (3)$$

Where, $NDVI_{MAX}$ and $NDVI_{MIN}$ are the maximum and minimum NDVI values of the study area, respectively. Based on the heat radiation transfer equation, the mono window algorithm has been developed to prepare the land surface temperature image from the Landsat thermal band data. This algorithm needs three parameters, i.e. emissivity, atmospheric transport and average effective atmospheric temperature. The mono window is calculated as follows (Qin *et al.*, 2001; Sobrino *et al.*, 2004):

$$T = \frac{1}{C[a(1-C-D)+(b(1-C-D)+C+D)Ts-DTa]} \quad (4)$$

Where, Ts is the effective temperature of the satellite and Ta is the average atmospheric temperature, which can be obtained with a simple relationship with the temperature near the earth (To). The coefficients a and b have the constant values of -67.355351 and 0.458606 respectively.

The variables C and D are obtained from the following equations (Sobrino *et al.*, 2004).

$$C = t\varepsilon \tag{5}$$

$$D = (1-t)[1+(1-\varepsilon)t] \tag{6}$$

Where, t is the atmospheric transfer, which can be estimated using land surface temperature and water vapor data, as well as regional meteorological observations. According to the findings, there is always a linear relationship between t and water vapor (Zhang *et al.*, 2007). Finally, T is the LST resulting from the mono-window algorithm using the thermal data of the Landsat satellite, which is used in this study to monitor the LST.

- **Spatial statistical analysis of LST**

Spatial data in environmental studies refers to the observations that are highly impacted by the location of these observations in the studied space. The spatial correlation between these data is an obstacle to the usual statistical methods. For this reason, spatial statistics is used as a suitable method to analyze these data. Spatial analysis can monitor temporal and spatial changes of spatial data well in an area (Khosravi *et al.*, 2016).

It is very important to know the pattern governing the spatial data, thus before any analysis and preparation of the map, spatial autocorrelation analysis should be done in order to check the distribution of data in space (Chen *et al.*, 2009). In this study, spatial autocorrelation analysis (global and local Moran's model) and hot spots or Getis-Ord-Gi index (GI) were used to investigate the spatial pattern governing the LST in the study areas from 1985 to 2020. The global Moran's spatial autocorrelation analysis only determines the type of pattern, thus, the local Moran was used to show the spatial distribution of the surface temperature pattern in the studied cities. Cluster and non-cluster analysis, which is known as the Anselin Local Moran's I statistic, is an optimal model for representing the statistical distribution of phenomena in space (Waagepetersen & Schweder, 2006). For this purpose, to cluster and non-cluster analysis and in each feature in the information layer, the Z-score and P-Value, which express the significance of the calculated index, were calculated based on the following relationship (Anselin, 1995; Zhang *et al.*, 2008; Anselin *et al.*, 2009):

$$Ii = \frac{xi-\overline{x}}{S_x^2} \sum_{i=1\ j\neq i}^{n} \omega_{ij}\,(xi-\overline{x}) \tag{7}$$

Where, xi is the feature of the ith complication and $\overline{x}$ is the average of the relevant characteristic, ω (ij) is the spatial weight of the i and j complications, and the value of si is calculated using the following equation (Anselin, 1995; Anselin *et al.*, 2009)

$$S_i = \left[\frac{n^2\sum_{i=1}^{n}\sum_{j=1}^{n}W_{ij}^2+3\left(\sum_{i=1}^{n}\sum_{j=1}^{n}W_{ij}\right)^2-n\sum_{i=1}^{n}\left(\sum_{j=1}^{n}W_{ij}\right)^2}{(n^2-1)\times\left(\sum_{i=1}^{n}\sum_{j=1}^{n}W_{ij}\right)^2}\right]^{0.5} \tag{8}$$

Where, n is the total number of complications in the layer, Wij is the spatial weight between complications i and j, which is the reciprocal of the distance between two complications. Also, the standard Z score is obtained from the following equation (Anselin, 1995; Anselin *et al.*, 2009):

$$Z_{Ii} = \frac{I_i}{\sqrt{V[I_i]}} \tag{9}$$

$$V[I_i] = E[I_i^2] - E[I_i]^2 \quad (10)$$

Where, if the value of I is positive, it means that the desired complication is surrounded by similar complications. Therefore, the desired complication is a part of that cluster, and if the value of I is negative, it means that the desired complication is surrounded by dissimilar complications (Dadashi and Fallah, 2014).

Based on the local Moran index, the regions with positive spatial autocorrelation (maximum clusters) and the regions with negative spatial autocorrelation (minimum clusters) are identified. In addition to the results obtained from the local Moran's index, hot spot analysis can be used to validate the areas with high and low value clusters. In the analysis of hot spots, the Getis-Ord-Gi index is also used for all features in the data (Reynolds *et al.*, 2016). The calculated Z-score shows the regions in which the data are clustered with low or high values. The conceptual framework of this model works in such a way that a hot spot feature is considered when the feature itself and the features surrounding it are statistically significant. The Z score will be obtained when the local sum of the feature and its neighbors is relatively compared with the total sum of the features (Xunqiang *et al.*, 2011). This index is obtained from the following equation (Getis and Ord, 1992; Ord and Getis, 1995):

$$G_i^* = \frac{\sum_{j=1}^{n} W_{ij}^2 - \overline{x \sum_{I=1}^{n} W_{IJ}}}{S \times \sqrt{\frac{\left[n \sum_{j=1}^{n} W_{ij}^2 - \left(\sum_{j=1}^{n} W_{ij}\right)^2\right]}{n-1}}} \quad (11)$$

Also, the following equation is used to calculate S (Getis and Ord, 1992; Ord and Getis, 1995):

$$S = \sqrt{\frac{\sum_{i=1}^{n} x_j^2}{n} - (\overline{x})^2} \quad (12)$$

The Gi* is considered as a kind of Z score, therefore Z index is not calculated. The positive values of this index that are statistically significant, the higher they are, indicate proper clustering and the creation of hot spots (heat islands). The smaller the negative score of this statistically significant index means the clustering of low values and they form cold spots (Askari, 2019).

3. Results

Land use/ land cover maps extracted from satellite images provide basic information for managing and monitoring environmental systems (Kazemi *et al.*, 2018). Figure 2 shows the land use maps of Mashhad and Sari city related to specific time periods. The results of the validation of land use maps for each time period are also given in Table 4, and the acreage of each land use is shown in Figure 3.

After extracting land use maps, land use changes were also calculated using the LCM model in TerrSet2020 software, which are shown in Figure 4.

- **LST monitoring**

After extracting land use changes, extracting the LST in the desired time period was carried using the mono window algorithm within the Google Earth Engine platform. The LST maps of the two study areas are illustrated in Figure 5. Based on the obtained results, an average temperature increase between 1 to 2 °C was seen in the cities of Mashhad and Sari during the years 1985 to 2020.

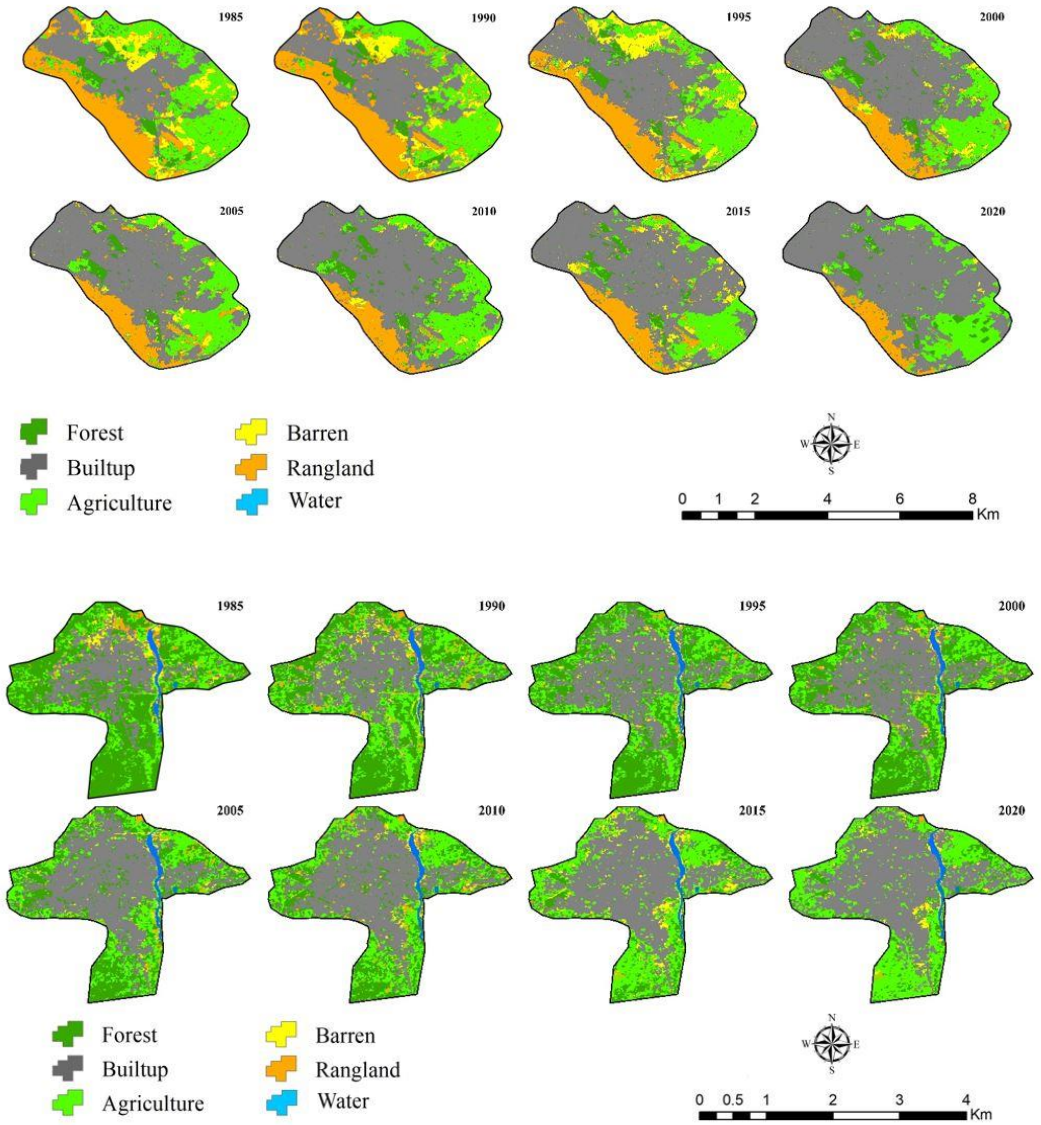

Fig. 2. Land use maps of Mashhad and Sari during the 8 studied periods

Table 4. Classification accuracy of land use maps of Mashhad and Sari cities during the 8 studied periods

	MASHHAD		SARI	
	Overall accuracy	Kappa	Overall accuracy	Kappa
1985	0.927	0.896	0.901	0.871
1990	0.894	0.851	0.913	0.884
1995	0.912	0.883	0.922	0.898
2000	0.912	0.877	0.926	0.902
2005	9.919	0.892	0.924	0.90
2010	0.91	0.89	0.953	0.935
2015	0.969	0.951	0.968	0.967
2020	0.942	0.924	0.966	0.963

- **Spatial statistical analysis of LST**

Moran's and local Moran's indices were used to show the spatial distribution of the pattern governing the surface temperature of the studied areas (Figure 6). The results of the local Moran's index are shown in Figure 7. Figure 8 shows the average results obtained from the the local Moran index (spatial autocorrelation) during 8 periods in all types of land uses.

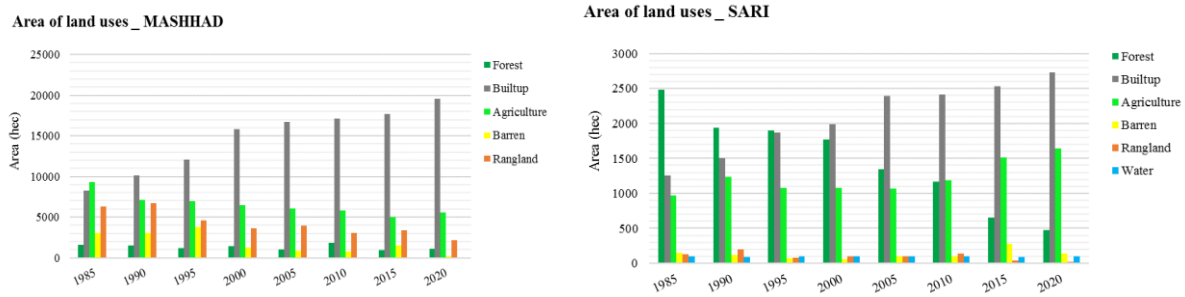

Fig. 3. Land use acreage for Mashhad and Sari cities during the 8 studied periods

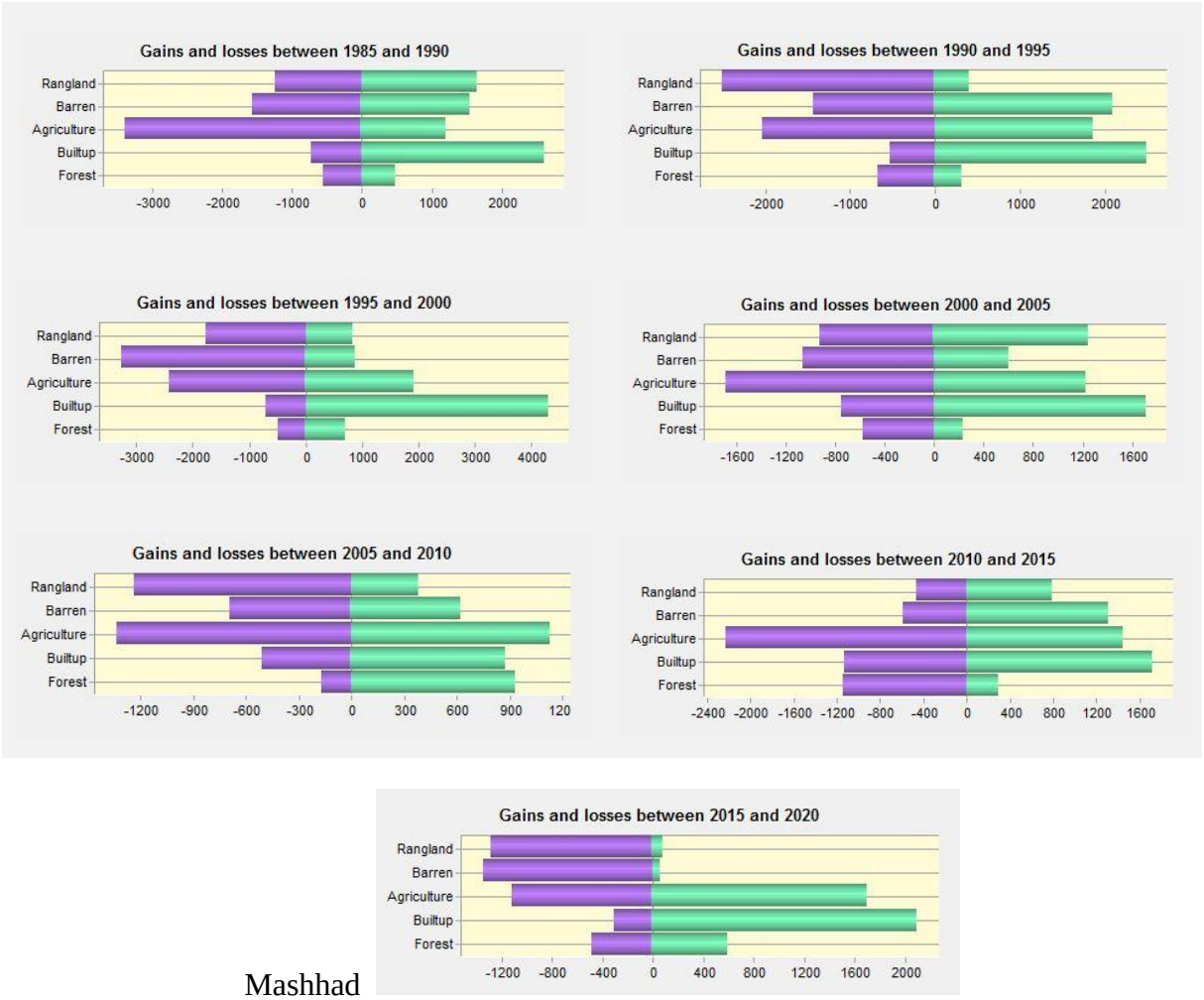

Mashhad

Fig. 4. The increase and decrease of land use areas in Mashhad and Sari during the 8 studied periods (in hectares)

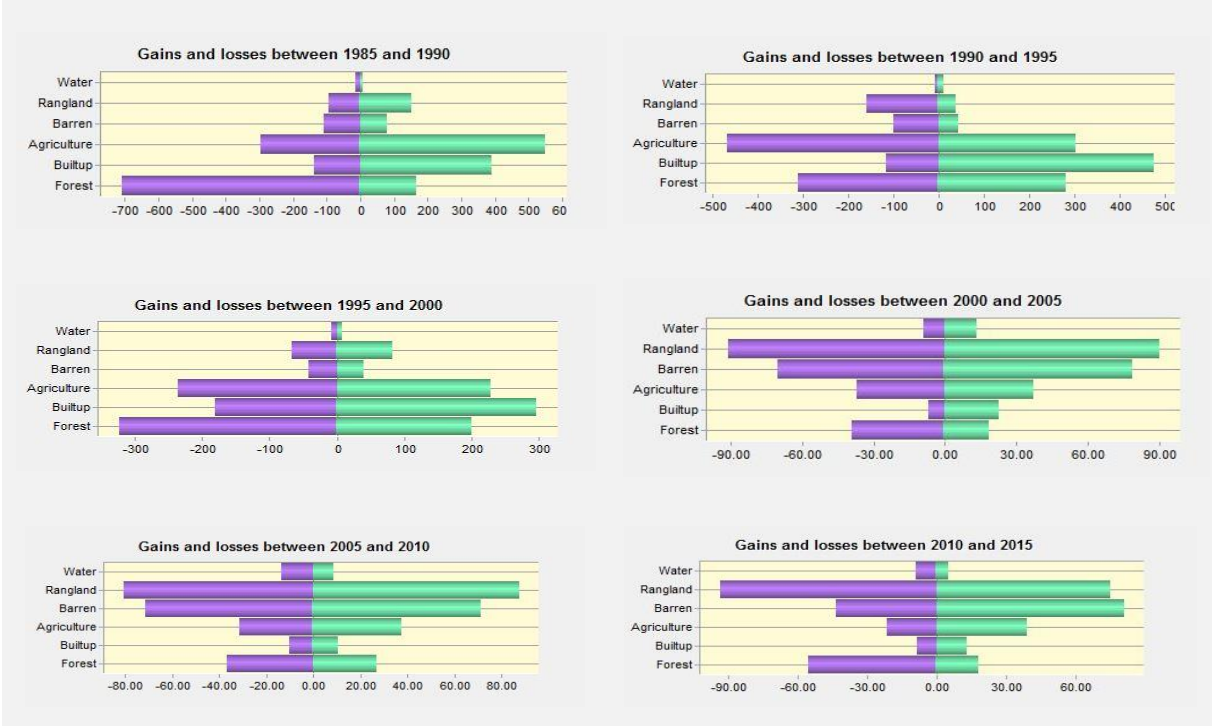

Sari

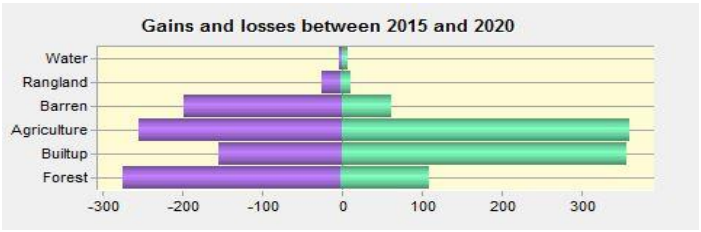

Fig. 4. Continued

In order to validate the results of the local Moran's index and the identified areas with high and low value clusters, the Getis-Ord-Gi index was used to analyze the hot spots. In this index, a Z-score is calculated in which the regions of data are clustered with a high or low value. (Figure 9).

Figure 10 shows the results obtained from the average distribution of the pattern of hot and cold spots in all types of uses. Also, in Figure 11 shows the average increase in temperature in the cities of Mashhad and Sari in different land use.

The results of increase of average temperature for different types of land use changes formed in Mashhad in the studied areas are shown in Figure 12.

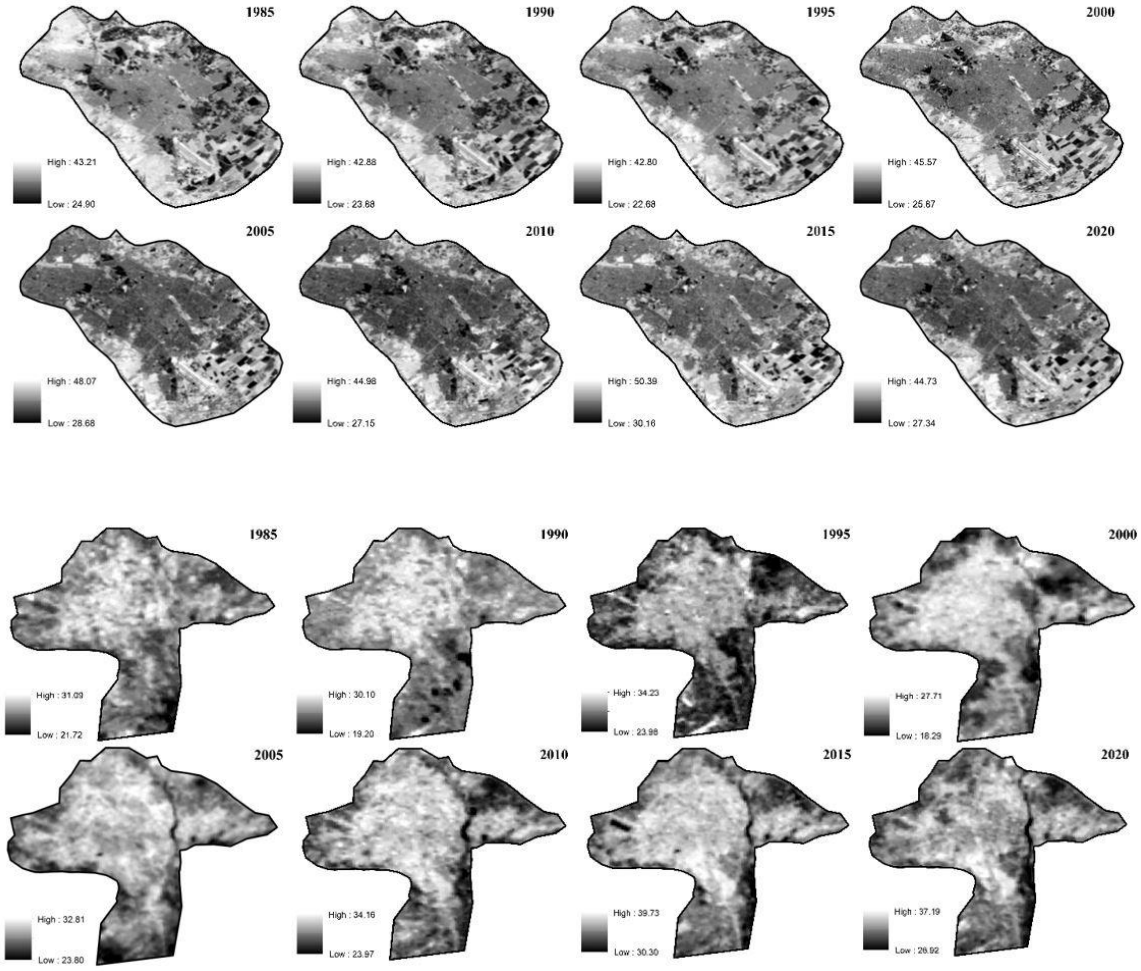

Fig. 5. LST map of Mashhad and Sari during the 8 studied periods

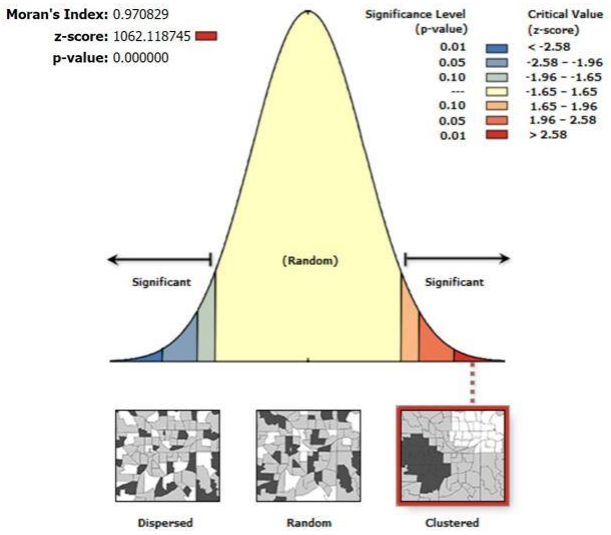

Fig. 6. Autocorrelation analysis results of the LST obtained from the Moran's index

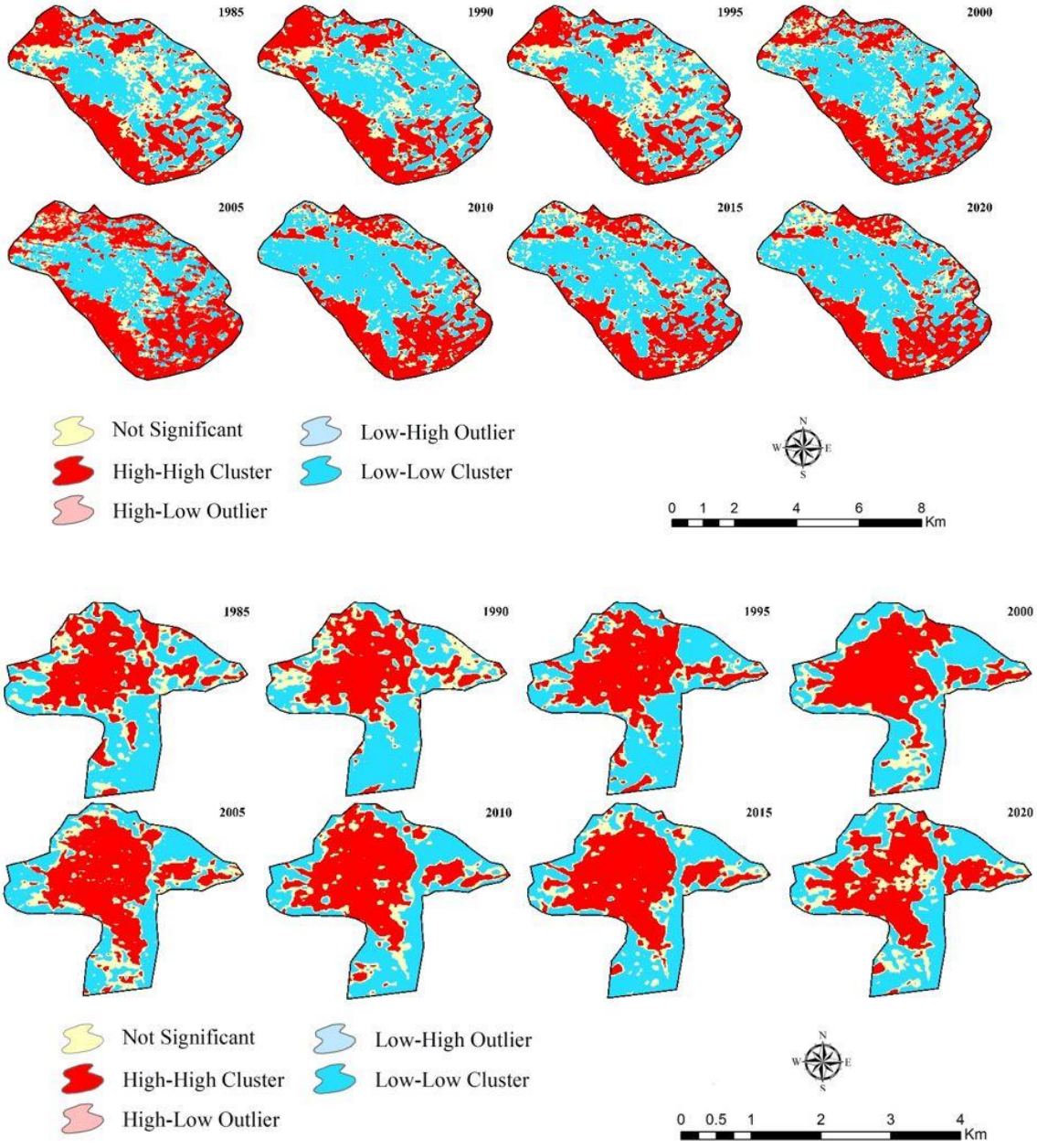

Fig. 7. The results of the local Moran model (spatial autocorrelation) of Mashhad and Sari city during the 8 studied periods

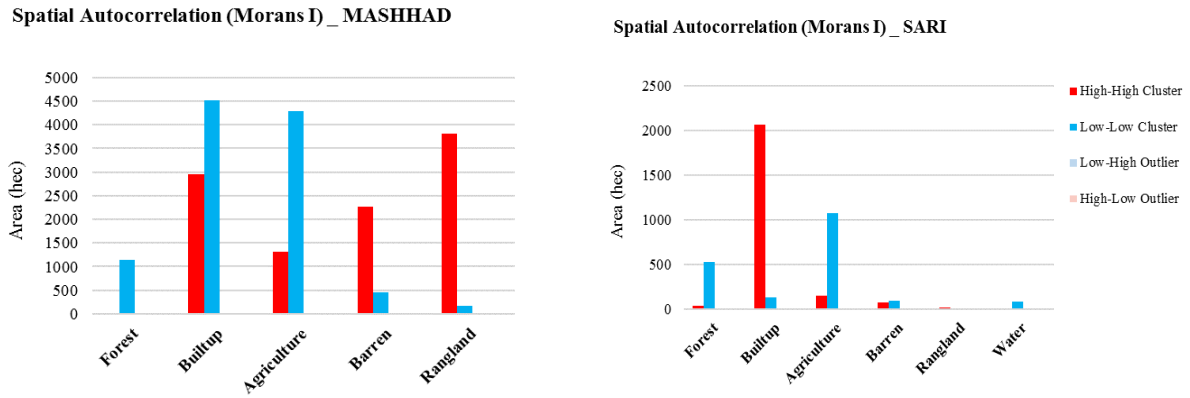

Fig. 8. The average results of the local Moran index (spatial autocorrelation) during 8 periods.

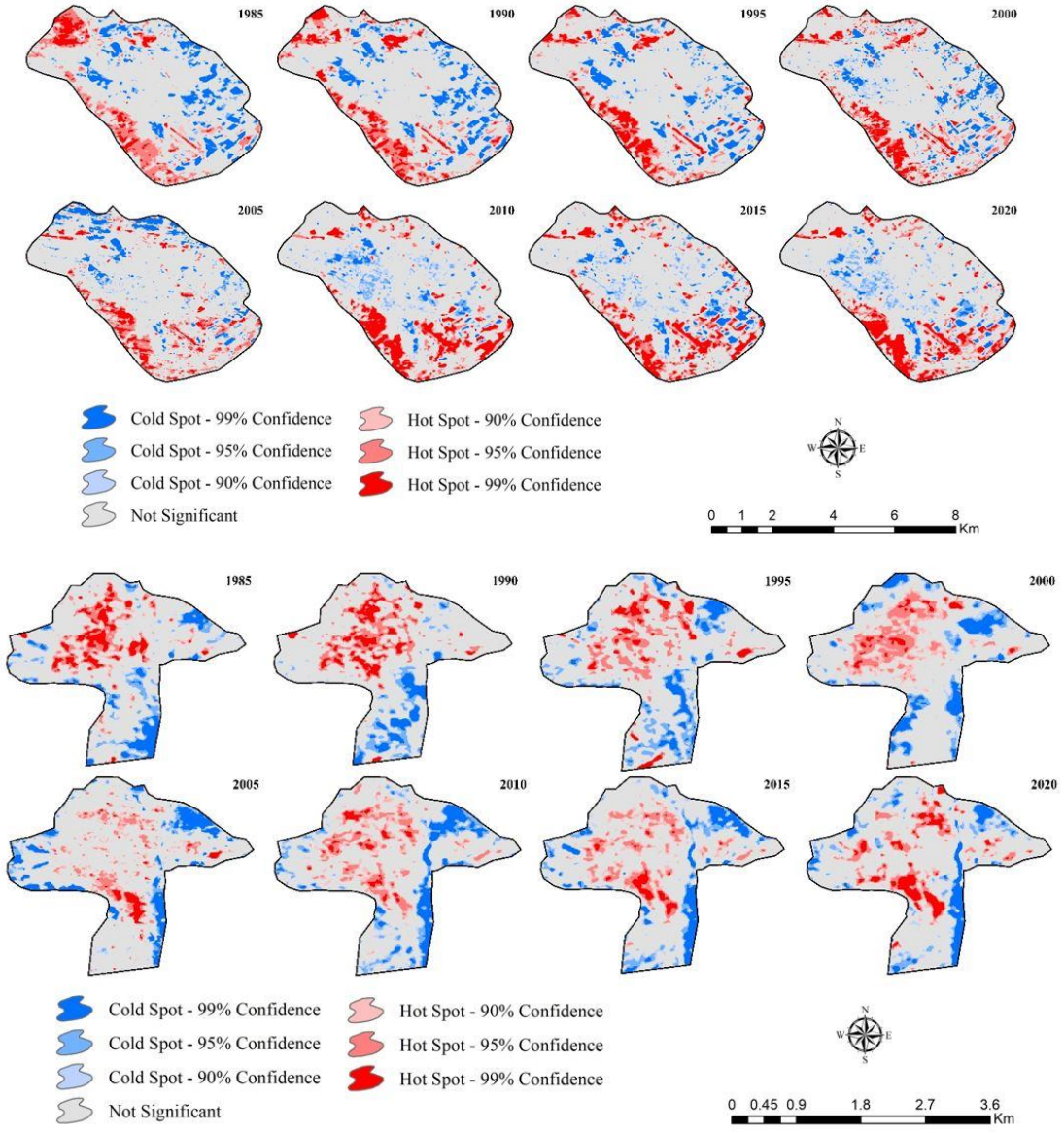

Fig. 9. The results of Getis-Ord-Gi index of Mashhad and Sari city

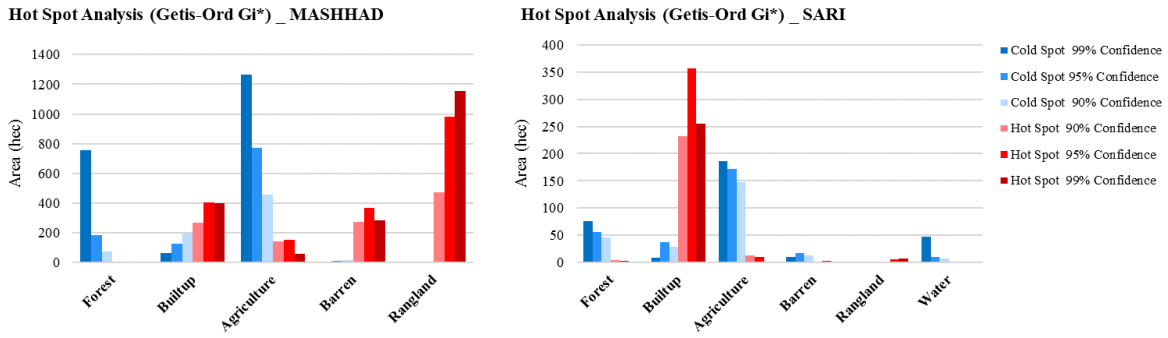

Fig. 10. The average results of Getis-Ord-Gi index of the studied areas

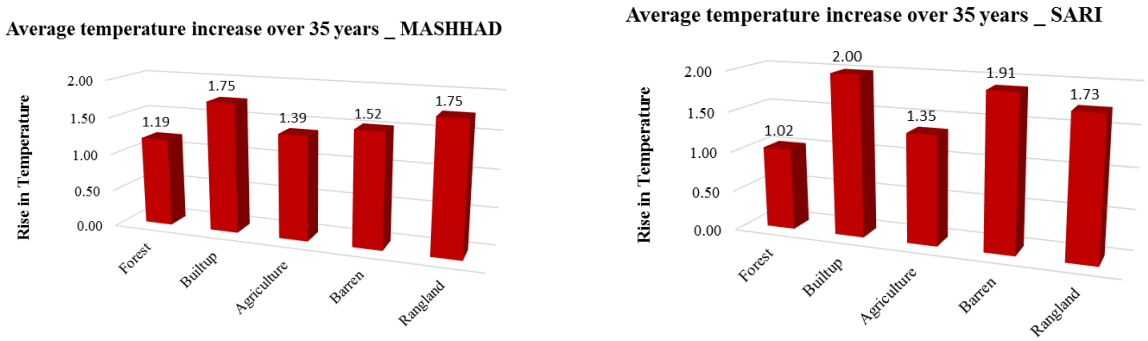

Fig. 11. The average increase in temperature in the cities of Mashhad and Sari in different land use

4. Discussion

In this research, in order to monitor and investigate the relationship between LST and land use, Landsat imageries dated 1985 to 2020 were used through the Google Earth Engine system. Land use/ land cover maps extracted from satellite images provide basic information for managing and monitoring environmental systems (Kazemi *et al.*, 2018). For this purpose, the object-oriented method based on the SVM algorithm was employed for the two studied areas in 8 time steps. In order to classify images three processing stages, i.e. pre-processing including radiometric and atmospheric corrections and contrast enhancement in the Landsat level 1 data, choosing the correct classification method based on the quantitative assessment of classification accuracy and finally post-processing including the use of Majority/Minority filters, were accomplished. As it is clear from the figure 4, the largest area in 1985 for the study area of Mashhad belongs to agriculture and for the study area of Sari, it belongs to forests. However in 2020, these land uses have been greatly reduced and the largest acreage belongs to built-up category. This increase in the land use acreage of built-up areas at the same time as the decrease in the land use acreage of agriculture and forests shows a clear direction of the sprawl of cities and their progress within these land uses.

Land surface temperature is considered one of the most important effective parameters in global studies, which is an important factor in controlling the biological, chemical and physical processes of the earth (Alavipanah, 2016). One of the most basic environmental problems is the increase in LST and the creation of heat islands in the areas that have been transformed into cities or metropolises without management (Alavipanah *et al.*, 2013).

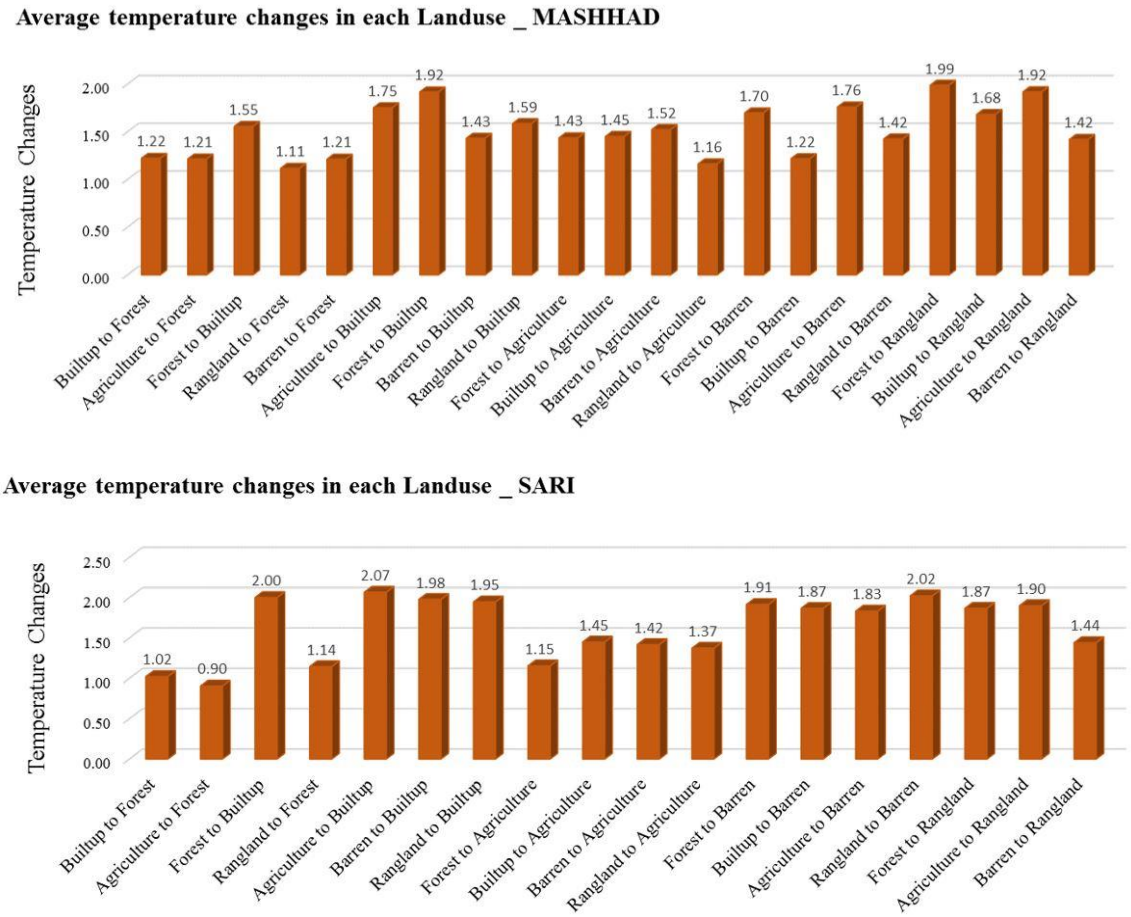

Fig. 12. The increase of average temperature for different types of land use changes formed in Mashhad and Sari

Since in environmental studies we often face observations that are not independent of each other and their dependence on each other is caused by the location of the observations in the studied space, recognizing patterns governing spatial data is very important (Singh *et al.*, 2017). Moran's and local Moran's indices were used to show the spatial distribution of the pattern governing the surface temperature of the studied areas. The results of this analysis show that the distribution of features is in the scattered, random and clustered forms. The Moran's index closer to positive 1 means that the data have spatial autocorrelation and a cluster pattern, and the closer to negative 1 means the data have a scattered and discrete pattern. Cluster mapping tools are used to display the distribution pattern of spatial data on the map. The local Moran's index and Getis-Ord-Gi index are among these tools. From the local Moran's index, where the result is displayed spatially on the map, if the value of the I index is positive, the desired feature is surrounded by similar features, so it is a part of the cluster, and if it is negative, it is surrounded by dissimilar features. The index value is calculated by the standard score and the P-Value can be interpreted. In this index, High-High values indicate clusters of high values (Hot) or positive autocorrelation (with a 99% confidence level), and High-Low values indicate non-clustering, where a large value is surrounded by a small value; and vice versa in the Low-High values, the low-value feature is surrounded by the high-value features, and finally the Low-Low values indicate clusters with negative spatial autocorrelation or low (Cold) values.

The results of the local Moran's index showed that in both study areas the changes of the spatial correlation of the surface temperature are significant with a high level of confidence

(with cluster dispersion at the level of 99% and 95% confidence), which is consistent with the results of similar studies (Zandi *et al.*, 2023; Shi *et al.*, 2017). However, the formation process of hot spots in study areas with different climate conditions were different. In hot and dry areas, the formation of hot clusters with a confidence level of 99% has taken place in the Rangelands and barren lands, and as a result, heat islands have been located in these areas. The rangelands have a maximum temperature compared to built-up areas (based on LST maps); thus have more High-High clusters assigned to them compared to the cities. These results are consistent with similar research conducted on heat islands in hot and dry regions, which show a reverse trend of heat islands in these regions, such that the areas around the city have a higher surface temperature than the central areas of the city. This is due to the presence of barren soil around the city, which heats up quickly during the day, and on the contrary, surface cold islands are created in the city (Lazzarini *et al.*, 2013; Rasool *et al.*, 2015). And based on the obtained results and visual comparison of hot spots and their related land uses, it has been determined that in temperate and humid climate, hot clusters are also in built-up areas. However, in hot and dry climate, hot spots are located in Rangelands and cold spots are located in agricultural lands and water bodies. These findings are consistent with the results of the local Moran's index. Also in Getis-Ord-Gi index index, each feature is considered in the framework of the features that are located in its neighborhood, and it is considered as a hot spot feature that both feature and its neighbors are statistically significant. For positive and statistically significant Z-scores, the larger the Z-score means that high values are clustered to a large extent and form hot spots, and for statistically significant negative Z-scores, the smaller the Z-score means that more severe clustering occurred at low values and formed cold spots

Based on the results obtained from the average distribution of the pattern of hot and cold spots (Fig 15), it was revealed that the pattern of spots in areas with hot and dry climate is also different from the temperate and humid climate using the Getis-Ord-Gi index. The rangelands have more hot High-High clusters than built-up areas due to having maximum temperatures (based on LST maps). These results are also consistent with the studies of Hashemi *et al.* (2018). They demonstrated that the heat islands of urban surfaces have spatial, daily and seasonal fluctuations, which is one of the effective factors in the daily spatial changes of the LST, and also the difference in the reaction of different land covers to the equal sunlight reaching the surface. In hot and dry areas due to the presence of soil and barren lands around the cities, a negative heat island (urban Cold Island) is observed during the day.

Therefore, based on the results obtained and matching the maps of the LST and the maps resulting from the identification of hot spots obtained from the of Getis-Ord-Gi and local Moran's index using daily satellite imageries, in the areas with moderate conditions of Caspian climate, the highest temperature and hot spots are also formed in built-up areas. However, in hot and dry regions, rangeland areas outside the urban area have the highest temperature and hot spots. Thus, in order to investigate heat islands, it is suggested to use night images in these areas of the city, but the trend of temperature changes can be investigated by using daily imageries (Sadeghinia *et al.*, 2013).

Monitoring the LST (Fig 16) showed an increase in temperature between 1 to 2°C in all types of uses during 35 years. In general, the increasing trend of temperature in Sari metropolitan was more than in Mashhad metropolitan, so that Sari faced a temperature increase of 2°C during the studied period, while the maximum temperature increase in Mashhad city was 1.75°C. Moreover, by matching the average LST with the land use dynamics during the study periods, it was found that the increasing trend is different in different types of land uses. The increase in temperature in the built-up areas was estimated to be 2 and 1.75°C respectively in the cities of Sari and Mashhad. Accordingly, the average temperature of the three months of

summer in the city of Mashhad in the built-up areas enlarged from 34.5°C to 36.25°C and in the city of Sari has reached 31.51°C from 29.51°C. Furthermore, the increasing trend of temperature in rangelands of Sari and Mashhad is 1.91°C and 1.75°C, respectively. The minimum increase of temperature has occurred in lands with forest use, which is an increase of 1.02°C and 1.19°C for Sari and Mashhad, respectively. In both climate zones, the areas that changes have been in the direction of reducing or eliminating vegetation (such as changing the land use from forests and agricultural lands to built-up areas and barren lands and rangelands), the increasing trend of temperature is maximum. Conversely, the areas where the changes have been in the direction of increasing forests and agricultural lands, the increasing trend of temperature has been minimized.

5. Conclusion

In this research, the changes in spatial autocorrelation pattern of LST and its relationship with land use have been monitored in two metropolitans of Mashhad and Sari, Iran. For this purpose, temperature and land use maps were extracted during a period of 35 years using Google Earth Engine system, and then spatial autocorrelation maps of LST were extracted from the local Moran's and Getis-Ord-Gi indices. The results of consistency analysis obtained from the temperature maps and the indices employed in spatial statistics and also their spatial autocorrelation monitoring shows the appropriateness of using these indices in the spatial monitoring of LST.

The results proved the increasing trend of temperature between 1°C to 2°C in all types of land use according to the type of changes in land use. This increasing trend works differently in different classes and changes formed, so that the temperature increase in built-up lands was estimated to be 2 and 1.75 degrees Celsius in the cities of Sari and Mashhad, respectively. The average temperature of the three months of summer in Mashhad city in built-up areas has increased from 34.5°C to 36.25°C and in Sari city from 29.51°C to 31.51°C. while the minimum increase in temperature has occurred in the lands with forest coverage, which is 1.02°C and 1.19°C, respectively in the cities of Sari and Mashhad. Conclusively, in both climatic regions, the areas where the changes were in the direction of reducing or eliminating vegetation and creating residential areas, the temperature increase trend is the maximum, and the areas where the changes were in the direction of increasing forests and agricultural lands, the temperature increase trend is the minimum. Therefore, considering this important, and monitoring changes in the spatial autocorrelation pattern of the LST, can be used in planning and making the right policies for the formation of urban development process and paying attention to the creation of urban green spaces with proper distribution. Finally, it is suggested to combine the results to land use change modeling with different scenarios for the future years, and then by comparing the results in each region, take steps for proper management and sustainable development in urban areas.

References

Abdi, Komeil Kamyabi, S. Zandmghaddam, M.Z. 2020. Investigating the role of urban green space coverage on the trend of surface temperature changes in urban environments (case study: Sari city). Environmental Science and Technology Quarterly. 23(2). 135-146. (In Persian)

Abdul Athick, M.; Shankar, K. & Raja Naqvi, H. 2019. Data on time series analysis of land surface temperature variation in response to vegetation indices in twelve Wereda of Ethiopia using mono window. split window algorithm and spectral radiance model. Data in brief 27 (2019) 1047732.

Agarwal, S., Vailshery, LS,, Jaganmohan, M., Nagendra, H., 2013. Mapping urban tree species using very high resolution satellite imagery: comparing pixel-based and object-based approaches. ISPRS International Journal of Geo-Information 2:220-236.

Alavipanah, S. K. Hashemi Dare Badami, S. Kazemzadeh, A. 2014. Temporal-spatial analysis of the thermal island of Mashhad city according to the expansion of the city and land use-cover changes. Urban planning geography researches. 3(1). 1-17. (In Persian)

Alavipanah, S. K., Mansourmoghaddam, M., Gomeh, Z., Galehban, E., & Hamzeh, S. (2022). The reciprocal effect of global warming and climatic change (new perspective): A review. Desert, 27(2), 291-305.

Alavipanah, S.K. 2013. Principles of remote sensing and interpretation of aerial photos and satellite images. Second edition, Tehran, Tehran University (In Persian)

Alavipanah, S.K. 2016. Thermal remote sensing and its application in earth sciences. Second edition, Tehran, Tehran University (In Persian)

Amiri R., Q. Weng, A. Alimohammadi, and S. K. Alavipanah, "Spatial–temporal dynamics of land surface temperature in relation to fractional vegetation cover and land use/cover in the Tabriz urban area, Iran," Remote sensing of environment, vol. 113, no. 12, pp. 2606-2617, 2009.

Anselin L (1995) Local indicators of spatial association: LISA. Geogr Anal 27(2):93-115.

Anselin L, Syabri I, Kho Y (2009) GeoDa: an introduction to spatial data analysis. In Fischer MM, Getis A (eds) Handbook of applied spatial analysis. Springer, Berlin,Heidelberg and New York, pp.73-89.

Asghari Saraskanroud, Syed and Emami, Hadi. 2018. Land surface temperature monitoring and land use relationship with surface temperature using OLI and ETM+ sensor images, case study: Ardabil city. Applied Research Journal of Geographical Sciences, 19 (53). (In Persian)

Askari, A. 2011. Spatial statistics analysis using ArcGIS, publications of Tehran Municipality Information and Communication Technology Organization. 128 pages.

Becker, F., & Li, Z. -L. (1990). Temperature independent spectral indices in thermal infrared bands. Remote Sensing of Environment, 32, 17– 33.

Carlson, T. N., & Ripley, D. A. (1997). On the relation between NDVI, fractional vegetation cover, and leaf area index. Remote Sensing of Environment, 62, 241– 252.

Chen Q, Changjian N, Zhan L, Jingxuan R. 2009. Urban heat island effect research in Chengdu city based on MODIS data. In: 2009 3rd International Conference on Bioinformatics and Biomedical Engineering. IEEE, pp 1-5.

Dadashi Rudbari, A. A., A. Falah Qalhari, 2014. Analyzing the autocorrelation of Iran's seasonal rainfall using APHRODITE rainfall database. Journals of Applied Meteorology, 2(1): 47-53. (In Persian)

Estoque, R. C., Murayama, Y., & Myint, S. W. 2017. Effects of landscape composition and pattern on land surface temperature: An urban heat island study in the megacities of Southeast Asia. Science of the Total Environment, 577, 349-359.

Feng Y., C. Gao, X. Tong, S. Chen, Z. Lei, and J. Wang, "Spatial patterns of land surface temperature and their influencing factors: a case study in Suzhou, China," Remote Sensing, vol. 11, no. 2, p. 182, 2019.

Gao, Y., Mas J.F., and Navarrete A., 2009, The Improvement of an Object-oriented Classification Using Multi-Temporal MODIS EVI Satellite Data, International Journal of Digital Earth, Volume 2, Issue 3 September 2009 , PP. 219 - 236.

Getis A, Ord JK (1992), the analysis of spatial association by use of distance statistics.Geogr Anal 24(3):189-206.

Gorelick N., M. Hancher, M. Dixon, S. Ilyushchenko, D. Thau, and R. Moore, "Google Earth Engine: Planetary-scale geospatial analysis for everyone," Remote Sensing of Environment, vol. 202, pp. 18-27, 2017.

H. Yang and Y. Liu, "A satellite remote sensing based assessment of urban heat island in Lanzhou city, northwest China," International Archives of Photogrammetry. Netherlands: Remote Sensing and Spatial Information Sciences, 2005.

H. Yang and Y. Liu, "A satellite remote sensing based assessment of urban heat island in Lanzhou city, northwest China," International Archives of Photogrammetry. Netherlands: Remote Sensing and Spatial Information Sciences, 2005.

Hamzeh, S, Mijani, Naeem, and K. Firoozjaei, "Modeling the Relationship between Surface Temperature, Topographic Conditions, and Vegetation Using Landsat 8 Satellite Images," Natural Geography Research, vol. 50, no. 1, pp. 35-55, 2018. (In Persian)

Hashemidarebadami, Darvishi-Bulrani. A, Alavipanah, S.K, Maleki, Bayat. 2013. Analysis of heat island changes of urban surfaces during the day and night using MODIS multi-temporal products (case study: Tehran metropolis). Applied Research of Geographical Sciences. 52(19), 113-128. (In Persian)

He J., W. Zhao, A. Li, F. Wen, and D. Yu, "The impact of the terrain effect on land surface temperature variation based on Landsat-8 observations in mountainous areas," International Journal of Remote Sensing, vol. 40, no. 5-6, pp. 1808-1827, 2019.

Kazemi, M. Nafarzadegan, A. Mohammadi, F. 2018. Investigating the effect of land use changes on the thermal islands of Minab sity using random forest classification and spatial autocorrelation analysis. Journal of remote sensing and geographic information system in natural resources. 10(4) (In Persian)

Khosravi, Y., M. A. Heydari, A. Tawakli and A. A. a Zamani. 2016. Analysis of the temporal relationship between the surface temperature and the spatial pattern of land use changes (case study of Zanjan city). Jornal of Space planning and design. 21(3), 119-144. (In Persian)

Kotchi S. O., N. Barrette, A. A. Viau, J.-D. Jang, V. Gond, and M. A. Mostafavi, "Estimation and uncertainty assessment of surface microclimate indicators at local scale using airborne infrared thermography and multispectral imagery," Geospatial Technology–Environmental and Social Applications. Intech Publishers, Rijeka, Croatia, pp. 99-141, 2016.

Kumar L. and O. Mutanga, "Google Earth Engine applications since inception: Usage, trends, and potential," Remote Sensing, vol. 10, no. 10, p. 1509, 2018.

Lazzarini, M., Marpu, P. R., & Ghedira, H. (2013). Temperature-land cover interactions: the inversion of urban heat island phenomenon in desert city areas. Remote Sensing of Environment, 130, 136-152.

Li, M., Ma, L., Blaschke, T., Cheng, L., Tiede, D., 2016. A systematic comparison of different object-based classification techniques using high spatial resolution imagery in agricultural environments. International Journal of Applied Earth Observation and Geoinformation, 49, 87-98.

Mackie, R.I., 2013, Dynamic Analysis of Structures on Multicore Computers – Achieving Efficiency Through Object Oriented Design, Advances in Engineering Software 66, PP. 3–9.

Memarian, H., Balasundram, S.K. and Khosla, R., 2013. Comparison between pixel-and object-based image classification of a tropical landscape using Système Pour l'Observation de la Terre-5 imagery. *Journal of Applied Remote Sensing*, *7*(1), pp.073512-073512.

Mutanga O. and L. Kumar, "Google Earth Engine Applications," ed: Multidisciplinary Digital Publishing Institute, 2019.

Nascetti, M. Di Rita, R. Ravanelli, M. Amicuzi, S. Esposito, and M. Crespi, "free global dsm assessment on large scale areas exploiting the potentialities of the innovative google earth engine platform,"International Archives of the Photogrammetry, Remote Sensing & Spatial Information Sciences, vol. 42, 2017.

Ord JK, Getis A (1995) Local spatial autocorrelation statistics: distributional issues and anapplication. Geogr Anal 27(4):287-306.

Owen T., T. Carlson, and R. Gillies, "An assessment of satellite remotely-sensed land cover parameters in quantitatively describing the climatic effect of urbanization," International journal of remote sensing, vol. 19, no. 9, pp. 1663-1681, 1998.

Petropoulos, G.P., Kalaitzidis, C. and Vadrevu, K.P., 2012, Suppsrt Vector Machines and Object-based Classification for Obtaining Land-use/cover Cartography from Hyperion Hyperspectral Imagery, Computers & Geosciences, 41, PP. 99–107.

Puissant, A., Rougier, S., Stumpf, A., 2014, Object-oriented Mapping of Urban Trees Using Random Forest Classifiers, International Journal of Applied Earth Observation and Geoinformation, 26, PP. 235–245.

Qin, Z., Karnieli, A., & Berliner, P. (2001). A mono-window algorithm for retrieving land surface temperature from Landsat TM data and its application to the Israel–Egypt border region. International Journal of Remote Sensing, 22(18), 3719–3746.

Rasul, A., Balzter, H., & Smith, C. (2015). Spatial variation of the daytime surface urban cool island during the dry season in Erbil, Iraqi Kurdistan, from Landsat 8. Urban Climate, 14, 176-186.

Ravanelli R. *et al.*, "Monitoring the Impact of Land Cover Change on Surface Urban Heat Island through Google Earth Engine: Proposal of a Global Methodology, First Applications and Problems," Remote Sensing, vol. 10, no. 9, p. 1488, 2018.

Reynolds J, Wesson K, Desbiez A, Ochoa- Quintero J, Leimgruber P. 2016. Using remote sensing and Random Forest to assess the conservation status of critical Cerrado Habitats in Mato Grosso do Sul, Brazil. Land, 5(2): 12-24.

Rongali, G.; Ashok Kumar, K.; Ashvani Kumar, G. & Rakesh, K. 2018. A Mono-Window Algorithm for Land Surface Temperature Estimation from Landsat 8 Thermal Infrared Sensor Data: A Case Study of the Beas River Basin. India. Pertanika J. Sci. & Technol. 26 (2): 829 – 840.

Rott H., "Physical principles and technical aspects of remote sensing," in Remote sensing in hydrology and water management: Springer, 2000, pp. 15-39.

Sadeghi Nia, A., Alijani, B. & Ziyaian Firouzabadi, P. 2012. Spatial-temporal analysis of the thermal island of Tehran metropolis using remote sensing and geographic information system. Geography and environmental hazards. 1(4), 1-17. (In Persian)

Shi Y., L. Katzschner, and E. Ng, "Modelling the fine-scale spatiotemporal pattern of urban heat island effect using land use regression approach in a megacity," Science of the Total Environment, vol. 618, pp. 891-904, 2018.

Sidhu N., E. Pebesma, and G. Câmara, "Using Google Earth Engine to detect land cover change: Singapore as a use case," European Journal of Remote Sensing, vol. 51, no. 1, pp. 486-500, 2018.

Singh P, Kikon N, Verma P. 2017. Impact of land use change and urbanization on urban heat island in Lucknow city, Central India. A remote sensing based estimate. Sustainable Cities and Society, 32: 100-114.

Sobrino J. A., F. Del Frate, M. Drusch, J. C. Jiménez-Muñoz, P. Manunta, and A. Regan, "Review of thermal infrared applications and requirements for future high-resolution sensors," IEEE Transactions on Geoscience and Remote Sensing, vol. 54, no. 5, pp. 2963-2972, 2016.

Sobrino J., C. Coll, and V. Caselles, "Atmospheric correction for land surface temperature using NOAA-11 AVHRR channels 4 and 5," Remote sensing of environment, vol. 38, no. 1, pp. 19-34, 1991.

Sobrino, J.A., Jiménez- Munoz, J.C., Paolinib, L., (2004). Land surface temperature retrieval from Landsat TM, Remote Sensing of Environment, Vol 90 (4), Pp 434-440.

Tajbakhsh, M., Memarian, H., & Shahrokhi, Y. (2016). Analyzing and modeling urban sprawl and land use changes in a developing city using a CA-Markovian approach. Global Journal of Environmental Science and Management, 2(4), 397-410.

Tan J., D. Yu, Q. Li, X. Tan, and W. Zhou, "Spatial relationship between land-use/land-cover change and land surface temperature in the Dongting Lake area, China," Scientific Reports, vol. 10, no. 1, pp. 1-9, 2020.

Tran, D. X. Pla, F.Latorre-Carmona, PedroMyint, S, M .Kieu, H.(2017). Characterizing the relationship between land use land cover change and land surface temperature. ISPRS Journal of Photogrammetry and Remote Sensing, 124, 119-132.

Waagepetersen R, Schweder T. 2006. Likelihoodbased inference for clustered line transect data. Journal of Agricultural, Biological, and Environmental Statistics, 11(3): 264.

Wang R., M. Cai, C. Ren, B. Bechtel, Y. Xu, and E. Ng, "Detecting multi-temporal land cover change and land surface temperature in Pearl River Delta by adopting local climate zone," Urban Climate, vol. 28, p. 100455, 2019.(a)

Wang Y.C., B. K. Hu, S. W. Myint, C.C. Feng, W. T. Chow, and P. F. Passy, "Patterns of land change and their potential impacts on land surface temperature change in Yangon, Myanmar," Science of the Total Environment, vol. 643, pp. 738-750, 2018.

Wang, M.; Zhang, Z.; Hu, T. & Liu, X. 2019. A practical single-channel algorithm for land surface temperature retrieval: Application to Landsat series data. Journal of Geophysical Research: Atmospheres. 124. 299–316. (b)

Xiao, R., Cao, W., Liu, Y. and Lu, B., 2022. The impacts of landscape patterns spatio-temporal changes on land surface temperature from a multi-scale perspective: A case study of the Yangtze River Delta. *Science of The Total Environment*, *821*, p.153381.

Xunqiang M, Chen C, Fuqun Z, Hongyuan L. 2011. Study on temporal and spatial variation of the urban heat island based on Landsat TM/ETM+ in central city and Binhai New Area of Tianjin. In: 2011 International Conference on Multimedia Technology. IEEE, pp 4616-4622.

Yan, G., 2003. Pixel Based and Object Oriented Image for Coal Fire Research, http://www.ITC.com (accessed in July 2008). pp. 3-99.

Zandi, R., Salmani Moghadam, M., & Roki, Z. (2023). Measuring the Degree of Spatial Autocorrelation of Land Surface Temperature with Land Use (Isfahan City). Geography and Environmental Planning, 34(1), 61-76.

Zehrakar, Z., Shahidi, A., Memarian Khalilabad, H. 2019. Comparing the accuracy of pixel-based and object-oriented methods in land use classification (case study: Samalqhan Basin). Natural Environment, Natural Resources of Iran, 73(4), 687-700. (In Persian)

Zhang C, Luo L, Xu W, Ledwith V. 2008. Use of local Moran's I and GIS to identify pollution hotspots of Pb in urban soils of Galway, Ireland. Sci Total Environ 398 (1-3):212-221.

Zhang J., Y. Li, and Y. Wang, "Monitoring the urban heat island and the spatial expansion: using thermal remote sensing image of ETM+ band6," in Geoinformatics 2007: Remotely Sensed Data and Information, 2007, vol. 6752, p. 67522F: International Society for Optics and Photonics.